Appl Phys A (2013) 112:647–661
DOI 10.1007/s00339-013-7600-z

Applied Physics A
Materials Science & Processing

Quantum efficiency of technical metal photocathodes under laser irradiation of various wavelengths

F. Le Pimpec · C.J. Milne · C.P. Hauri · F. Ardana-Lamas

Received: 5 July 2012 / Accepted: 28 January 2013 / Published online: 14 February 2013

Abstract Quantum efficiency studies for various laser wavelengths and various technical metal surfaces were carried out in a dedicated unbaked vacuum chamber in the absence of a significant electrical field. Copper, magnesium, aluminum, and aluminum–lithium photocathodes were irradiated by two different high power, high repetition rate, laser systems. We have observed an emission of electrons for photon energies below the work function of the material. This is explained by multiple photon absorption by the photocathode. We have not observed any degradation of the QE for these materials, but an improvement when irradiating them over a long period of time. This is contrary to observations made in RF photoguns.

1 Introduction

In a free electron laser accelerator (FEL), one of the key components is the electron source. The source should provide a sufficient amount of electrons and should have a low emittance to enable the facility to provide the X-ray photons requested by the end users. The electrons can be produced by thermionic emission, photoemission or by field emission [1–4]. The successful operation [5, 6] of the first X-ray FEL (XFEL) Linac Coherent Light Source (LCLS) using a Cu photocathode has led the Paul Scherrer Institute (PSI) to adapt the LCLS gun design for the future SwissFEL facility [7, 8].

F. Le Pimpec (✉) · C.J. Milne · C.P. Hauri · F. Ardana-Lamas
Paul Scherrer Institute, 5232 Villigen, Switzerland
e-mail: frederic.le.pimpec@xfel.eu

C.J. Milne · C.P. Hauri · F. Ardana-Lamas
Ecole Polytechnique Fédérale de Lausanne, 1015 Lausanne, Switzerland

In the meantime, an injector test facility has been commissioned at PSI with an RF photogun using a diamond milled oxygen free electrolytic (OFE) Cu photocathode [9] as its electron source. The electron production is ensured by two different types of lasers, a Nd:YLF (Jaguar® by Time-Bandwidth [10]) and a broadband Ti:Sa (Pulsar® by Amplitude Technologies [11]) [12, 13]. In order to provide the required electron beam quality (emittance), it is necessary to provide a temporally and transversally shaped laser beam. This in turn has an impact on the available laser energy at the cathode, and this energy is needed to produce the amount of charge requested by the machine design [8]. The amount of charge produced by the cathode depends on its quantum efficiency (QE), which is defined as the number of electrons emitted per number of incident photons.

The performance and cost of an XFEL is ultimately driven by the emittance of the electron beam produced at its source. The smaller the emittance, the shorter the accelerator can be. In addition, the price of the laser used to extract the electrons from the cathode becomes potentially cheaper for cathodes with a high QE. This is true if one considers only the output of the laser energy at a given wavelength.

In a photocathode driven FEL, the thermal emittance can be minimized if the energy of the photons matches the work function of the material. If the condition is fulfilled, the QE of the cathode drops to zero. It is then of importance to know the work function of the photocathode used. Metallic photocathodes are very often exposed to air before their insertion in an RF gun, contrary to semiconductor photocathodes. The work function of such technical metals is then not known and is very different from clean metal surfaces.

One of the goals of this research, was to establish via the use of a laser with tuneable wavelength, the work function and the quantum efficiency of various potential metallic photocathodes for FEL accelerators. Potential alternatives to

copper are magnesium, aluminum, and aluminum–lithium. Yttrium has also shown its potential as a metal based cathode to replace copper [14, 15]. Despite the robustness of metallic cathodes, compared to semiconductor-type cathodes, aging is unavoidable. The aging of a cathode is translated into an unacceptable drop of QE for machine operation. Cathode aging is often reported during RF photogun operation [16]. This aging requires either in-situ repair (laser cleaning, ozone cleaning), to rejuvenate the QE of the cathode, or exchange of the photocathode [16].

The paper is organized as follows: description of the experimental setup (Sect. 2), QE measurements (Sect. 3), and exploration of aging (Sects. 4 and 5).

In Sect. 3, we have investigated the work function of two metallic photocathodes: copper and magnesium. Copper is one of the most used metals in warm accelerator technology, primarily due to its high electrical conductivity and its capacity to withhold rather high fields before arcing. Magnesium, which has demonstrated very good performances compared to copper in terms of QE and recently in emittance [17], still suffers from a lack of R&D to ensure its use as a photogun safe photocathode when exposed to a high field environment. The work function and QE were measured under different bias conditions, from 0 V to +12 V. This corresponds to a kV/m electrical field strength, at most. It is known that the application of a high electrical field is beneficial for the extraction of electrons first because of the Schottky effect, and secondly because it reduces beam expansion caused by intrabunch space charge forces. At this level of electrical field, the Schottky effect does not alter the net work function.

In a second experiment (Sects. 4 and 5), we have studied the aging of Cu in order to understand the effect of the laser irradiation on Cu in the absence of an intense RF field, in the order of 100 MV/m. The results obtained have led to a subsequent experiment: the aging study of various cathodes under exposure of a high repetition rate UV laser.

2 Experimental setup

The vacuum experimental system is shown in Fig. 1. The chamber is sealed by a transparent conflat MgF_2 vacuum window, 90 % transmission from 200 nm to 3000 nm. The chamber is pumped through a 50 l/s turbo pump and is not baked. The residual atmosphere is composed of water vapor for more than 95 %. The other noticeable peaks are 2 uma (hydrogen), 28 uma (mainly carbon monoxide), and 44 uma (carbon dioxide). The vacuum is monitored by a compact cold cathode gauge. The pressure during operation is between mid 10^{-5} Torr at the start of laser irradiation to mid 10^{-7} Torr after a few days of operation. The photocathode insert is placed at the center of the chamber and it is surrounded by a Cu Faraday cup (FC).

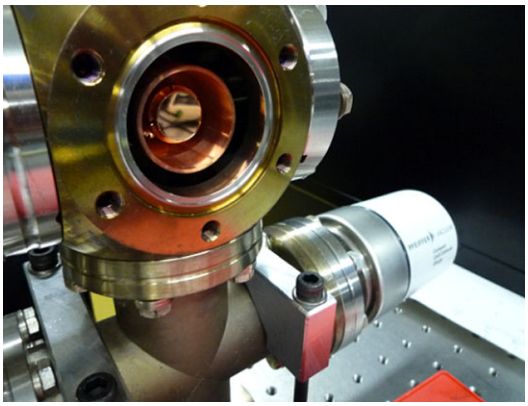

Fig. 1 Experimental vacuum chamber with a Cu cathode visible at its center surrounded by a Faraday cup (FC). A cold cathode compact vacuum gauge monitors the total pressure in the chamber. A conflat MgF_2 vacuum window seals the vacuum chamber

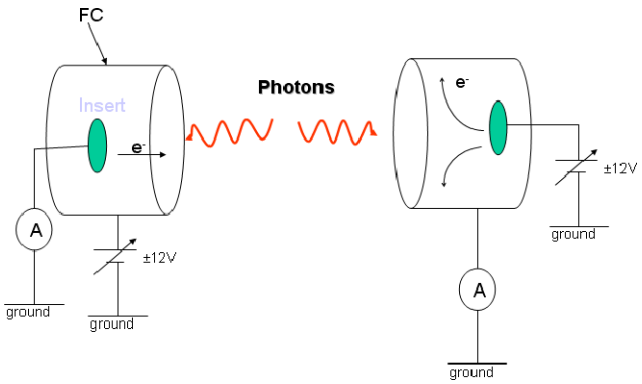

Fig. 2 Experimental setup, Electric diagram. The system encompasses an insert (photocathode) a Faraday cup (FC) surrounding it, a ±12 V battery powered power supply, and a K6514 Ammeter

The setup can be operated in two ways, shown in Fig. 2. Either by biasing the FC and recording the current leaving the insert using a Keithley® K6514 Ammeter, or by biasing negatively the insert and recording the current on the FC. A third option would have been to negatively bias the insert and record the current through the K6514; unfortunately, the K6514 cannot be used in a floating mode.

We have used two types of lasers: a Ti:Sa working at 800 nm wavelength, 100 fs pulse length with a 1 kHz repetition rate. The 800 nm pulses pump a Topas® [18] optical parametric amplifier (OPA) system, which allows the selection of various wavelengths (UV to IR). The fluence used was 86 μJ/cm^2 with a laser spot diameter between 2 to 3 mm. The laser peak intensity with these parameters was 0.856 GW/cm^2.

The second laser used was a Nd:YVO_4, Duetto® from Time-Bandwidth Products [10], working at 355 nm wavelength, with a 10 ps long pulse and a repetition rate set to 200 kHz. The laser average power was varied from 115 mW to 300 mW in order to extract more or less charge from

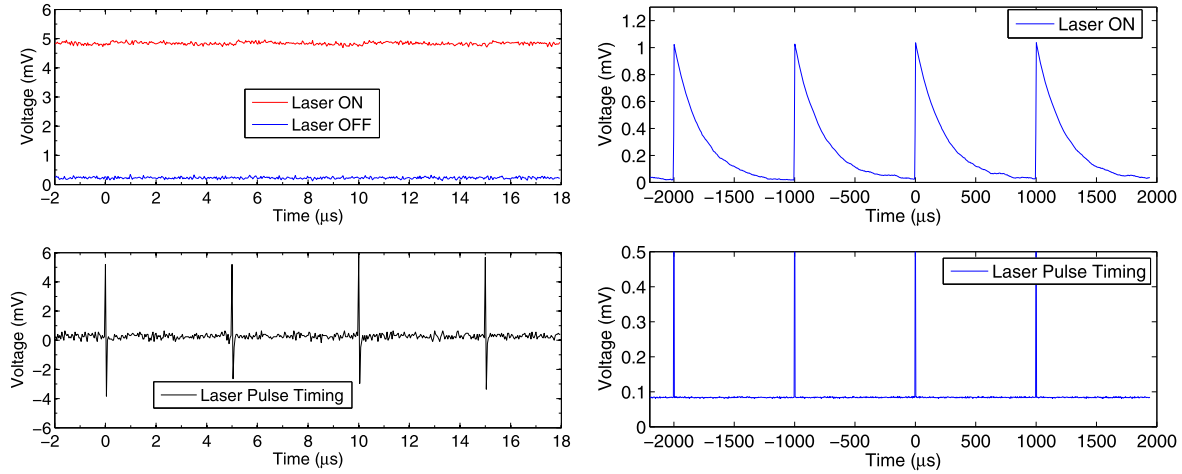

Fig. 3 The *left figure* (*top*) is the recorded voltage by the oscilloscope when the Mg cathode is illuminated by the Duetto® laser (355 nm, 200 kHz, 140 mW, ∼10 ps), FC = +9 V. A mV corresponding to a nA of photo-emitted current. The *right figure* (*top*) is the recorded voltage by the oscilloscope when irradiating the same polished Mg cathode using the Topas® laser (260 nm, 1 kHz, 5 μJ, ∼100 fs), FC is off. In both figures, the *bottom plots* are the traces of the recorded laser pulses

the various technical metals tested. The typical laser spot diameter on target was 8 mm. The laser fluences (peak intensity) were, respectively, 1.2 μJ/cm^2 (0.12 MW/cm^2) and 3 μJ/cm^2 (0.3 MW/cm^2). Both lasers produce linearly polarized light.

In order to cross-calibrate the K6514 Ammeter, we have measured the current coming from a freshly polished Mg cathode irradiated by the Duetto® laser (355 nm; 200 kHz; 140 mW) with a Tektronix-DPO 7254 oscilloscope, using the 1 MΩ entry impedance. The same cathode, kept under primary vacuum for 3 months, was also illuminated by the output from the Topas® which was set to (260 nm, 1 kHz, 5 μJ), Fig. 3.

The comparison shows excellent agreement between the K6514 reading 4.9 nA and the upper trace at 4.9 mV (laser ON) recorded by the oscilloscope, left figure top plot in Fig. 3. This 4.9 mV equates to a current of 4.9 nA. The associated QE is ∼0.023. The current read by the K6514 is similar, at the % level, when the FC power supply is switched off or when its voltage is set to 0 V via its potentiometer. A zoom in of the laser ON trace shows a small increase every 5 μs. This corresponds to the 200 kHz repetition rate of the laser (Fig. 3, left figure bottom plot). The oscilloscope cannot resolve the fast current signal produced by the 10 ps long laser pulse, due to the inherent impedance of the whole system. This includes the capacitance of the BNC cable. Consequently, the current displayed by the oscilloscope looks like a DC offset.

In the case of the Topas laser, right plot, the oscilloscope can resolve each pulse. The integrated signal (in nV s) for one pulse multiplied by the 1 kHz repetition rate is equal, within 5 %, to the current recorded by the K6514.

The measurement system is not fast enough to resolve the current for every pulse, which is commonly achieved in an accelerator. We hence define the QE as the number of electrons coming from the average current measured by the K6514 over the number of photons the laser produces in one pulse. A laser delivering 1 mW with 1 kHz repetition rate produces 1 μJ/pulse, and with a 200 kHz repetition rate, 5 nJ/pulse.

3 Magnesium and copper QE vs. wavelength

As already mentioned in the Sect. 1, the ultimate performance and cost of an FEL is determined by the emittance of the electrons emitted at the source. The intrinsic emittance or thermal emittance is the lowest limit in beam emittance that one can reach for a given cathode material, surface electric field, and laser wavelength. The intrinsic emittance can be expressed as follows, Eq. (1) [19]:

$$\varepsilon_{\text{thermal}} = \sigma_x \times \sqrt{\frac{h\nu - \Phi_0 + e^{3/2}\sqrt{\frac{E}{4\pi\epsilon_0}}}{3m_0c^2}} \tag{1}$$

where the parameters are in SI units: σ_x the horizontal RMS beam size, $h\nu$ the energy of the photons (J), Φ_0 the work function (WF) of a technical metal (J), which differs from an atomically clean surface, e the elementary charge, E the applied electric field (V/m), m_0 and ϵ_0 the rest mass of the electrons and the vacuum permittivity, respectively. The third term in the numerator of Eq. (1) is the reduction of the potential barrier due to the presence of the electric field (Schottky effect). An effective WF (Φ_{eff}) can be defined,

Table 1 Work function and associated wavelength for some bulk elements [20–24]

Material	Work function (eV)	Wavelength λ (nm)
Mg	3.66	339
Al	4.06–4.26	310–290
Cu	4.53–5.10	274–245
MgO	2.8	443
Al_2O_3	3.9	318
Cu_2O	5.2	239
CuO	5.3	234
Laser	4.74/4.67/3.49/2.48	262/266/355/500

Eq. (2),

$$\Phi_{\text{eff}} = \Phi_0 - e^{3/2}\sqrt{\frac{E}{4\pi\epsilon_0}} \tag{2}$$

In the absence of an external electric field, the best emittance is achieved when the photon energy matches the WF of the element. Unfortunately, when this condition is satisfied, the QE drops to zero [19]. From the literature, one can find various WF for different clean metals [20]. The WF of the metals is modified depending on their surface chemistry and crystallographic orientation. Table 1 shows some of the literature work functions for the bare metals we have tested and the associated wavelength (λ). To ensure the proper operation of a compact FEL like SwissFEL [8], it is necessary to know the WF of the cathode installed in order to produce an electron beam of acceptable emittance with the required amount of charge. This knowledge characterizes the reproducibility of the production process of the cathodes. In addition, this permits to reduce the cost of the gun laser as it allows to fix its characteristics (wavelength, power). Finally, this contributes to having a more stable gun laser as it becomes less complex to operate and to maintain compared to a fully tuneable laser system.

3.1 QE vs. wavelength—measuring the work function

We have measured the dependence of the QE as a function of wavelength, provided by the Topas® OPA, for polished and mirror like, Cu Fig. 4, and Mg Fig. 5. According to theory, we should see a sharp drop of the QE for $h\nu - \Phi_0 \sim 0$. During the first experiment the FC was not biased. The pressure during the experiment was in the low to mid 10^{-6} Torr. The QE data are compared to QE measurements obtained in a combined Diode-RF electron gun, labeled (OBLA) and using the RF photogun of the SwissFEL injector, labeled (Injctr).

We have repeated the experiment on Cu and Mg polished cathodes using two different laser pulse lengths. The natural pulse length of the Topas output is ∼100 fs. Using a quartz rod to stretch the pulse, the duration is increased to ∼1 ps. The results for the QE (λ) presented in Fig. 6 have been obtained with the FC set to +8 V. We have ensured the collection of all electrons emitted by setting properly the

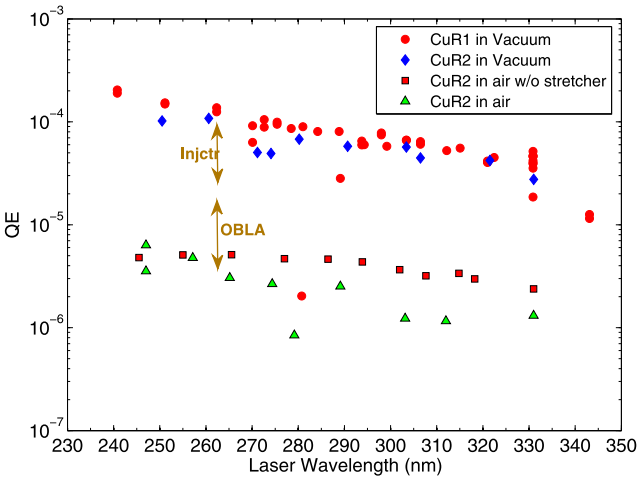

Fig. 4 QE vs. wavelength of two different polished (mirror like) Cu samples. The FC is unbiased. The QE are compared at a specific wavelength with QE data measured in two different accelerators

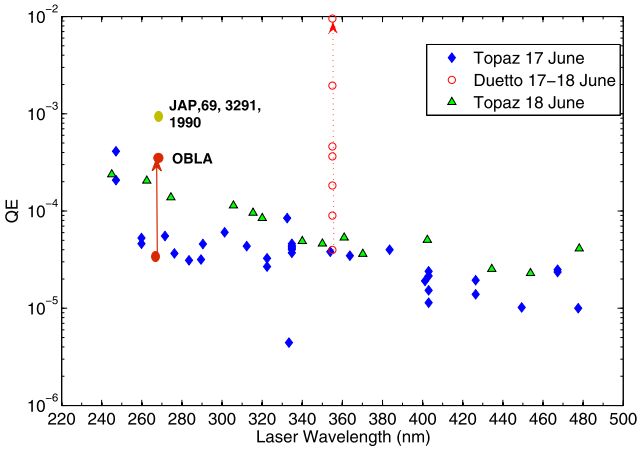

Fig. 5 QE vs. wavelength of polished (nonmirror-like) Mg#2. The FC is unbiased

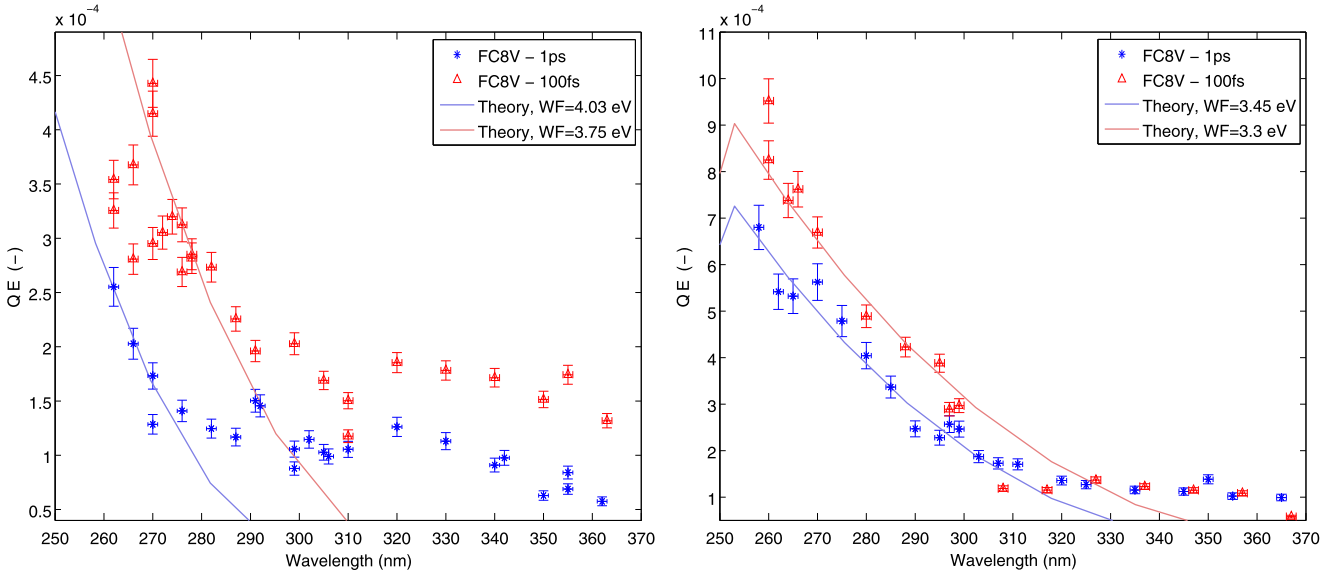

Fig. 6 QE vs. wavelength of a polished (mirror-like) Cu#R4 sample (*left plot*) and of a freshly repolished Mg#2 (*right plot*), using two laser pulse lengths 1 ps and 100 fs. The *straight lines* are fits to the data using Eq. (3)

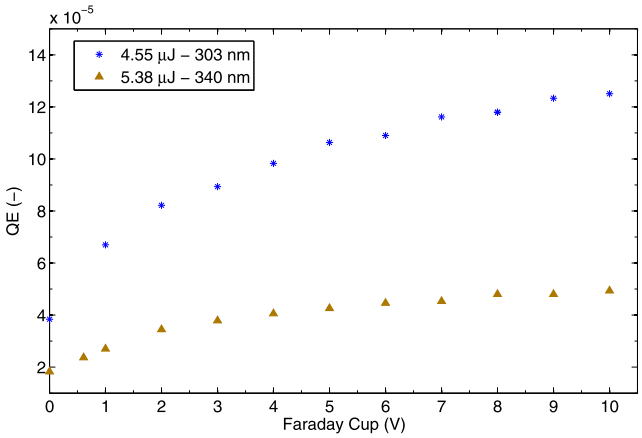

Fig. 7 QE of Cu#R4 vs. the FC voltage at fixed wavelength for a fixed Topas® energy in µJ

laser energy (in µJ) at a given wavelength (nm), as shown, for example, in Fig. 7.

3.2 Results above the WF

Using the photoemission model described by Spicer [25] and Eq. (3) for the QE(λ) [19, 26], we have tried to fit the measurements in Fig. 6.

$$QE(\omega) = \frac{1 - R(\omega)}{1 + \frac{\lambda_{\text{opt}}}{2\lambda_{e-e}(E_m)} \frac{E_{\text{ph}}\sqrt{\Phi_{\text{eff}}}}{E_m^{3/2}} \left(1 + \sqrt{\frac{\Phi_{\text{eff}}}{E_{\text{ph}}}}\right)} \times \frac{E_F + E_{\text{ph}}}{2E_{\text{ph}}} \times \left[1 - \sqrt{\frac{E_F + \Phi_{\text{eff}}}{E_F + E_{\text{ph}}}}\right]^2 \quad (3)$$

The validity of Eq. (3) implies that $\frac{E_F+\Phi_{\text{eff}}}{E_F+E_{\text{ph}}} < 1$, hence a photon energy above Φ_{eff}. The equation parameters are as follows. R is the reflectivity, E_F is the Fermi energy, $E_{\text{ph}} = \hbar\omega$ is the photon energy, λ_{opt} is the laser penetration depth, λ_{e-e} is the electron–electron scattering length and E_m is the energy above the Fermi level. Φ_{eff} is the effective work function, which is the work function Φ_0 of the bare material minus the barrier reduction due to the external field applied. In our case, no strong electric field is present on the cathode, hence $\Phi_{\text{eff}}\ (eV) \approx \Phi_0$ (see Eq. (2)).

The material reflectivity R and the optical penetration depth λ_{opt} are photon energy dependent. $\lambda_{\text{opt}} = \frac{\lambda}{4\pi k}$ with k being the imaginary part of the complex index of refraction. λ_{e-e} for Mg has been set equal to λ_{e-e} for Al. In the energy range considered for the escaping electron, the mean free path can vary sharply [27, 28].

The parameters used to fit the data for Cu and Mg are summarized in Table 2. For parameters varying as a function of the photon energy, a reference is given.

The fits are rather insensitive to the value of λ_{opt}. On the contrary, the fits are sensitive to the value of the mean free path λ_{e-e} and to the reflectivity (R). For Mg, there is a gap for R between 3 eV and 5 eV photon energy [20]. The fits shown in Fig. 6 (right plot) have been obtained for a constant reflectivity ($R = 0.72$). We have also extrapolated the reflectivity values between 3 and 5 eV. The fits using those values are no more correct. Fitting the data by utilizing Eq. (3) or the density of states of the material [29] will also show a discrepancy. This can be understood as Eq. (3) is obtained by making use of the free-electron gas model and by approximating the Fermi–Dirac distribution by a Heaviside distribution [19, 26].

Table 2 Parameters used to fit the QE data for Cu and Mg of Fig. 6 [20, 26]

Parameters	Cu	Mg
R	[20]	[20]
E_F	7 eV	7 eV
λ_{opt}	[20]	[20]
λ_{e-e}	2.2 nm	5 nm
E_m	8.6 eV	8.6 eV
Φ_0	3.75–4.03 eV	3.3–3.45 eV

Finally, the theory seems to fit relatively well the Mg photoemission by assuming a work function which is between the pure Mg metal and its oxide, Fig. 6 and Table 1. For Cu, Fig. 6 (left plot), one can fit well the data by using WF values below the clean Cu WF (up to 1 eV, Table 1). The meaning of such a fit could lead to the hypothesis that the Cu surface is contaminated by a chemical species like a hydride or an alkali. The Mg and Cu samples were installed in the same manner using the same ethanol cleaned tools and gloves. Contamination is unlikely to have occurred.

3.3 Results below the WF

We have observed that in all cases, the current recorded did not drop to the noise level of the K6514 when the wavelength of the laser was longer than the wavelength associated with the lowest WF of the clean elements; see Table 1. Sub-ps or ps duration laser pulses seem to affect the surface so that photoemission is possible for wavelengths longer than the photoemission wavelength threshold. When comparing the QE for Mg or Cu, at pulse lengths of 0.1 ps and 1 ps, the QE differs only a little, Fig. 6. Nevertheless, it seems interesting to look at different mechanisms, which could explain the electron emission at a photon energy below the material WF. Do we have:

- Thermal effects
- Plasmonic effects
- Multiphoton absorption
- Mechanical effects (stress, strain)
- Surface chemistry (oxide effect)

3.3.1 Thermal effects

The increase of temperature due to the laser irradiation of the inserts can be calculated using Eq. (4):

$$Q = m \times C_s \times \Delta T \tag{4}$$

where Q is the heat energy (J), C_s is the specific heat (J/(kg K)), and m the mass of the material (kg). We use at most 10 μJ of laser energy in the UV spectrum per pulse. We assume that all the laser energy is converted into heat.

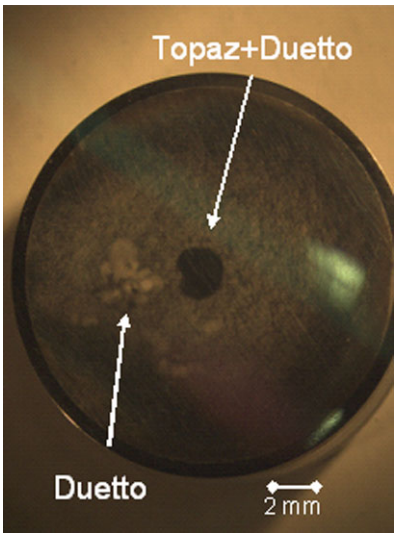

Fig. 8 Damages caused by laser exposure to polished but rough Mg# 2

The increase of temperature over the whole sample is given in column 4 of Table 3. In column 5 of Table 3, we have considered that the UV light ($\sim 5 \times 10^{15}$ Hz) heats only a very thin layer of the insert (skin depth) ~1 nm thick, and thus over the whole sample surface. If one assumes that only the skin depth under the irradiated area of the laser is heated, then the temperature increase will exceed 900 K, which is enough to melt Mg and Al. We have not observed any damage to polished mirror-like samples. The deposited laser energy dissipates quickly into different dissipative channels. The melting point of materials is linked to the lattice temperature, which is well described by a thermodynamic model. In this time scale, an electron-lattice model should be used to evaluate properly the end temperature of the lattice.

However, we have observed a dark spot under an optical microscope for the Mg, Fig. 8. This black spot can also be observed on Mg cathodes, which have undergone laser cleaning in the combined Diode-RF electron gun (OBLA) [14], Fig. 9. In the OBLA experiment, we have raster scanned the laser beam across the Mg surface. The laser fluence could be up to 40 mJ/cm^2 at 266 nm, using a 10 ps long laser pulse with a repetition rate of 10 Hz. The diamond shaped area cleaned, Fig. 9, was obtained using 12 mJ/cm^2 of laser fluence. In the small chamber experiment, the flu-

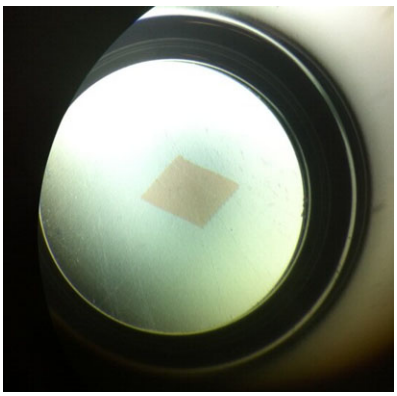

Fig. 9 Damage caused by laser cleaning on polished Mg in the combined Diode-RF gun (OBLA)

ence of the Topas® and Duetto® on Mg#2 were respectively less than 85 μJ/cm^2 (2–3 mm laser spot size) and 1.2 μJ/cm^2 (8 mm laser spot size).

From the discussion above, we conclude that thermal effects cannot account for the emission of electrons for laser energies below the work function.

3.3.2 Plasmon assisted photoemission

Surface plasmons can enhance the photoemission of surfaces [30–33]. The photoemission enhancement occurs for some angles of incidence and is also polarization dependent. We operate at normal incidence, and both lasers are linearly polarized in the plane of the photocathode. At normal incidence the probability of plasmon excitation is quasi null [31]. However, when surface roughness is on the order of a few 10's of nanometers, it is possible to excite surface plasmons. This would enhance the photoemission process [17]. The roughness of our polished samples was not measured. From previous measurement on similar cathodes, we believe that the average roughness is below 50 nm and above 10 nm, for mirror-polished cathodes.

3.3.3 Mechanical effects (stress, strain)

All of our inserts are mechanically polished. This induces stresses in the metal and on its surfaces. After polishing, the inserts are not baked, hence not stress relieved. Mechanical stress has been shown to modify the WF of metals [34]. However, the modification seems not to be sufficient to account for the photoemission of Cu at photon energies below 4.1 eV.

3.3.4 Surface chemistry

The presence of oxygen on the surface can significantly modify the WF of a bare metal, either by lowering it or by increasing it [21, 35, 36]. Although contaminant layers produced by air exposure are usually detrimental to the QE [15, 16], applying a thin film of MgO over silver cannot only lower the silver work function, but may also be beneficial for the electron beam emittance in an accelerator [37].

The beneficial influence of oxygen adsorbed on the surface has been shown previously [38, 39]. We believe that some part of the photoemission curve for Mg, Fig. 5, is explained by the presence of the oxide. On the contrary, natural copper oxide seems to have a work function above 5 eV [22].

It is interesting to note that Qian et al. [17] state that laser cleaning is efficient for removing contaminants, and cite MgO. Ozone cleaning will on the contrary oxidize the surface and restore a degraded QE [16]. However, no experiment shows how the oxide (hydride [40]) and the QE evolve in time under UV photon conditioning. A dedicated experiment using an X-ray photoelectron spectroscope (XPS) could answer such a question.

It is worth mentioning that in their paper Cashman and Huxford [38] quoted another experiment on Mg and that the conclusion was that the QE between 240 nm and 280 nm was exceptionally high, and that Mg would be of practical use up to 400 nm.

3.3.5 Multiphoton absorption

Multiphoton absorption, mainly two-photon absorption [41], is possible if the density of photons incident on the surface is high enough. Both the Topas® and Duetto® laser sources can deliver such intensities. Figure 10 shows the intensity of current extracted from Cu at 253 nm and at 331 nm for Topas® pulses of 100 fs and 1 ps.

For photon energies above the WF, like for $\lambda = 253$ nm, one expects a linear dependence of the current vs. the laser energy. For photon energy below the WF, for $\lambda = 331$ nm, one should see a quadratic dependence of the current vs. the laser energy. For Cu, at both wavelengths, we have a linear dependence of the current emission versus the laser energy for laser pulse length of 1 ps. For laser pulse lengths of 100 fs, the dependence seems quadratic. However, the quadratic dependence should be positive and not negative as measured. This negative dependence is often seen in RF photoguns when the bunch space charge hampers the emission of electrons [16]. A linear fit through zero can also be satisfactorily applied for Cu#R2 irradiated at 253 nm with a 100 fs laser pulse length. Such fit implies an electron emission by a one-photon photoelectric effect, which is nonspace charge limited.

For Mg#2, we have measured the current emission vs the laser energy. For $\lambda = 247$ nm the dependance is linear. For the following wavelength λ (403 nm, 520 nm), the dependance is quadratic with a positive curve, hence implying a photoelectric effect driven by a two-photon absorption.

Table 3 Temperature increase of the different metallic cathodes when exposed to 10 μJ/pulse laser irradiation

Metals	Mass (kg)	Specific heat (J/(kg K))	ΔT (K)	ΔT (∼1 nm) (K)
Cu	0.0028	387	9.2×10^{-6}	19
Mg	0.0021	1050	4.5×10^{-6}	23
Al	0.0014	900	7.9×10^{-6}	42

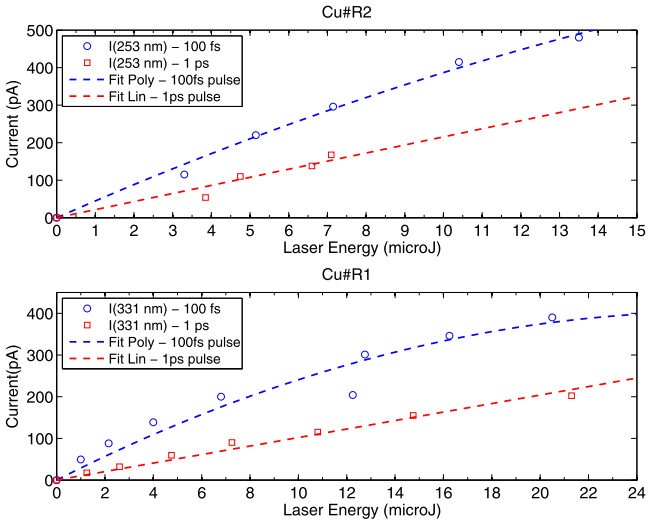

Fig. 10 Electron Current extracted versus the Topas® laser energy at 253 nm for CuR2 and at 331 nm for CuR1. In both cases, the FC is OFF

3.4 QE comparison with other data

For Cu photocathodes installed in photoguns, it is normal to find QE values in the 10^{-5} range. We measured similar values in our combined Diode-RF gun, labeled OBLA in Fig. 4, and in our RF photoinjector, labeled Injctr in Fig. 4. At 250 nm, QE values as high as 1.4×10^{-4} were also reported. This is consistent with our measurements [16, 42, 43].

We have also reported some of the QE data obtained on bulk or thin film Mg obtained in our combined Diode-RF gun, labeled OBLA, Fig. 5. The results obtained are comparable with literature data [15–17, 44].

Although it seems reassuring that the QE reported in the literature is compatible with the data obtained in this experiment, one should be careful in understanding how the QE has been derived. In a proper accelerator, the diagnostics measuring the charge are fast enough to measure the charge of each bunch. Usually, QE results obtained using a lamp or a laser are average measurements.

4 Aging of Cu in an RF photogun

LCLS has shown that a high current, XFEL-operation compatible emittance, can be obtained from a well-prepared Cu photocathode. A long lifetime between cathode exchange is also beneficial for user operation. However, as the cathode ages the QE drops. Figure 11 shows the evolution of the charge emitted by a Cu cathode after its installation and after months of operation. A localized charge drop is clearly visible on the right plot of Fig. 11. This corresponds to the location of the incident laser.

In-situ techniques, like laser cleaning, can be applied to regenerate the QE. On the right photograph of Fig. 8, we have seen how aggressive laser cleaning can modify the surface. Laser induced surface alteration was also seen on the Cu cathode of LCLS and in the SPARC experiment [16].

At the PSI injector, the UV lasers work at a low repetition rate (10 Hz). The two lasers used at the injector, Jaguar® or Pulsar®, are set to operate with a 10 ps long pulse, at a wavelength of $\lambda = 262$ nm or 270 nm. The laser spot size is 1 mm on target. The typical laser energy used to irradiate the photocathode is 10–20 μJ per pulse. The fluence varied from 1.27 to 2.55 mJ/cm^2 according to the laser spot size on target. The laser power density (or optical intensity [41]) was 127 to 255 MW/cm^2.

Figure 12 shows the QE evolution in time of one Cu cathode (Cu_3) and is compared to the QE of another Cu photocathode (Cu_1) after a year of operation in the PSI injector.

In order to reproduce the QE hole in the small system chamber, we have used the Topas® laser with the following settings: 1000 Hz repetition rate, 1 ps long pulse, $\lambda = 261$ nm, a laser spot size between 1 to 1.2 mm on target. The energy per pulse was 9 μJ so a fluence between 0.8 to 1.15 mJ/cm^2 and a power density between 800 to 1150 MW/cm^2. The QE and current measured during the laser exposure of a Cu insert are shown in Fig. 13. The already used Cu sample (CuR2) was installed after an ethanol wipe. The sample was exposed to the Duetto® laser 90 days before this experiment, and was stored in air during that time. Any exposure to air negates any effects from a laser conditioning/cleaning.

The Topas® was not available during nights, hence the gaps in the conditioning curve in Fig. 13. The injector operation is also usually stopped during nights. The overall time of the laser on target is ∼20 h. The fluence in the small chamber is, in the worst case, 70 % of the injector gun fluence. This amounts for an equal time of 58 days of injector operation. By that time, we should have seen a degradation of the QE and not an improvement as seen on the left plot of Fig. 13.

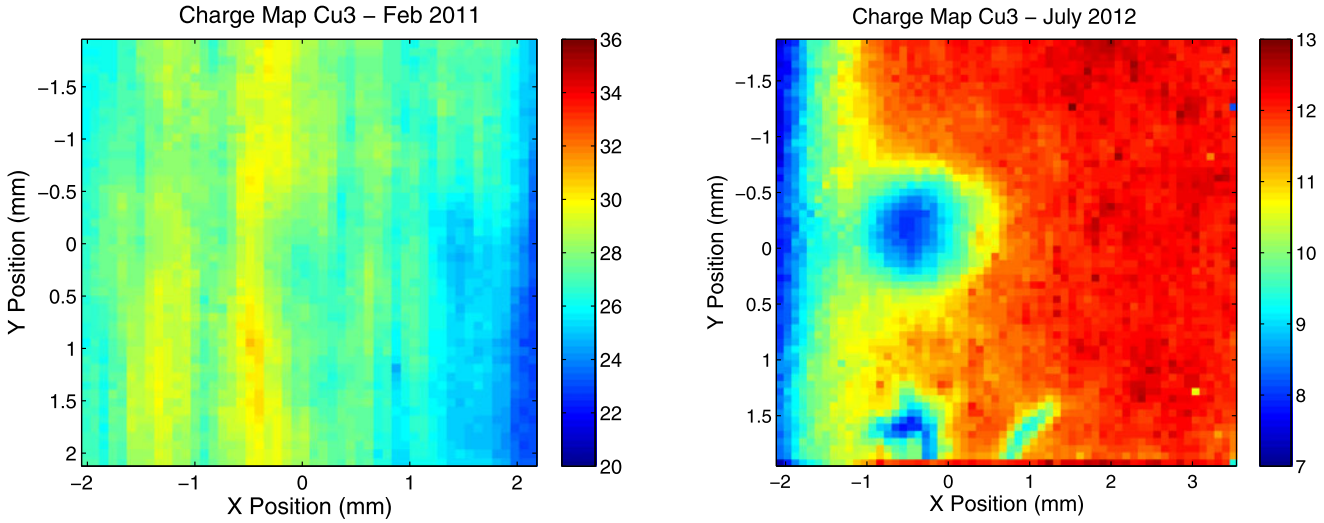

Fig. 11 Charge map (pC) evolution of the Cu photocathode. *Left plot*: initial charge map. *Right plot*: after 17 months of Injector operation

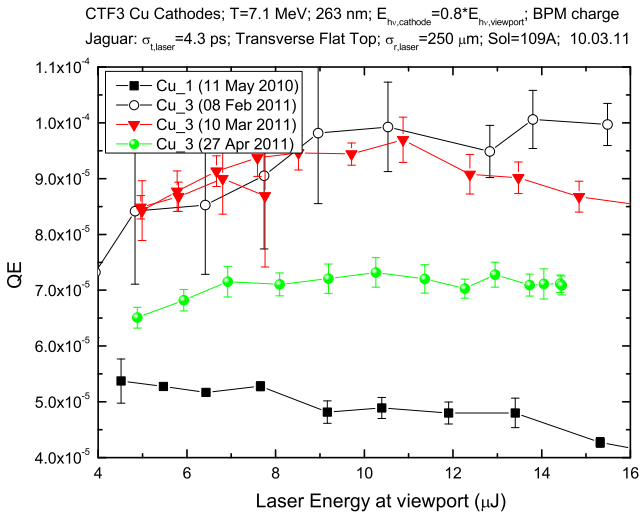

Fig. 12 New Cu photocathode (Cu_3) QE evolution after three months of injector operation. Comparison with the QE of the first cathode installed Cu_1 [45]

We then moved the laser spot to another location on the cathode and further reduced the laser spot size to 0.7 mm. The initial QE, $t = 2790$ min, is similar to the first starting point at $t = 0$ min. The QE did increase but then seemed to level off after a few hours of operation. The laser energy was constant to 10 μJ ± 1.5 μJ. The sample CuR2 showed no surface damage upon removal from the chamber.

We changed the sample to another Cu insert, which was also previously used and stored in air. We irradiated this sample using the Duetto® laser with its wavelength set to 266 nm, with 200 kHz repetition rate. The spot size was set to 0.4 mm in diameter, and the fluence used was decreased from initially 255 μJ/cm^2 to 65 μJ/cm^2. At high fluence, the sample produced up to 7 nA of current with the FC set at +4 V and a couple of nA with the FC unbiased. We probed a different location on the insert with a lower laser fluence. The laser beam size was sufficiently small to avoid any overlap on a previously irradiated area. Again, we saw no sign of QE degradation, but on the contrary, a QE increase even after three continuous days of irradiation at 200 kHz (266 nm).

We can only hypothesize about the reasons why we could not degrade the QE. Our RF photogun is baked to 120 °C during almost a week. Hence, a different vacuum spectrum than in an unbaked vacuum system. In the baked case, the vacuum spectrum is dominated by the hydrogen peak (2 uma) and not by water. The cathode in the electron gun is submitted to a high power (20 MW) and high gradient (100 MV/m) of RF field alternating at 3 GHz. This RF field produces dark current and ions. Both can impact the cathode and degrade the QE. However, Fig. 11 (right plot) still shows a mostly homogeneous QE over the whole cathode.

The vacuum environment of our system is at first dominated by water (>95 %). It is then possible that the intense laser light cracks the water molecules, producing very reactive radicals. These radicals would continuously restore the QE, as does an Ozone cleaning [16]. The pressure is usually in the 10^{-6} Torr range. At this pressure, a monolayer is formed every second. Laser heat can also activate surface molecule diffusion, and perhaps the rearrangement at this pressure of the oxide layer is beneficial, although the mechanisms are unclear. However, one should note that the vacuum spectrum of an unbaked system can be similar, qualitatively, to a baked system, if one allows the vacuum chamber to be pumped long enough.

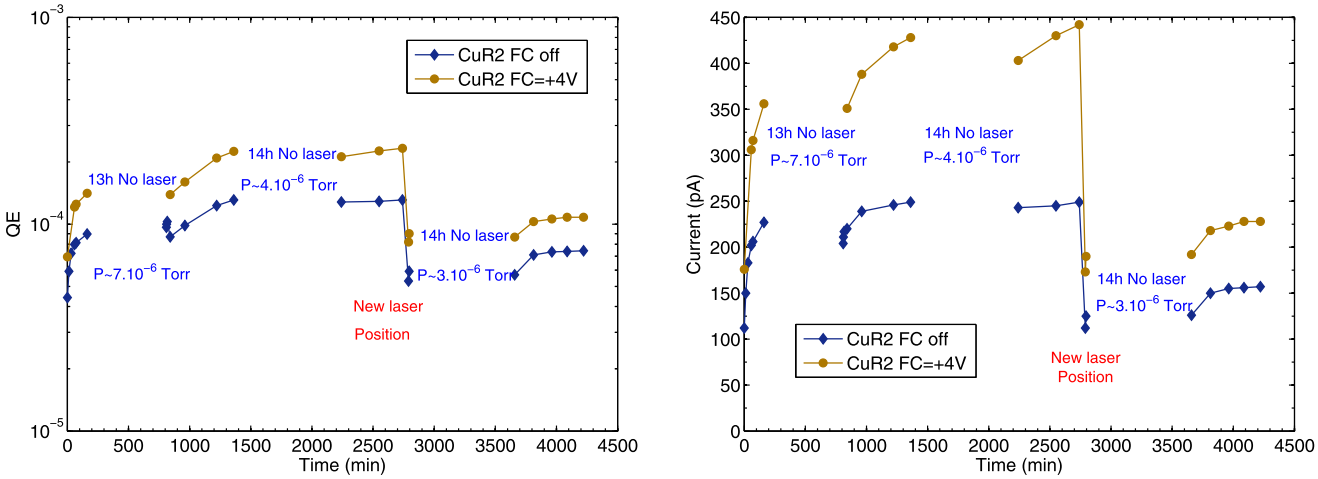

Fig. 13 QE (*left*) and Current (*right*) measured from a Cu cathode (CuR2) using the Topas® laser with a 1 kHz repetition rate and with $\lambda = 261$ nm

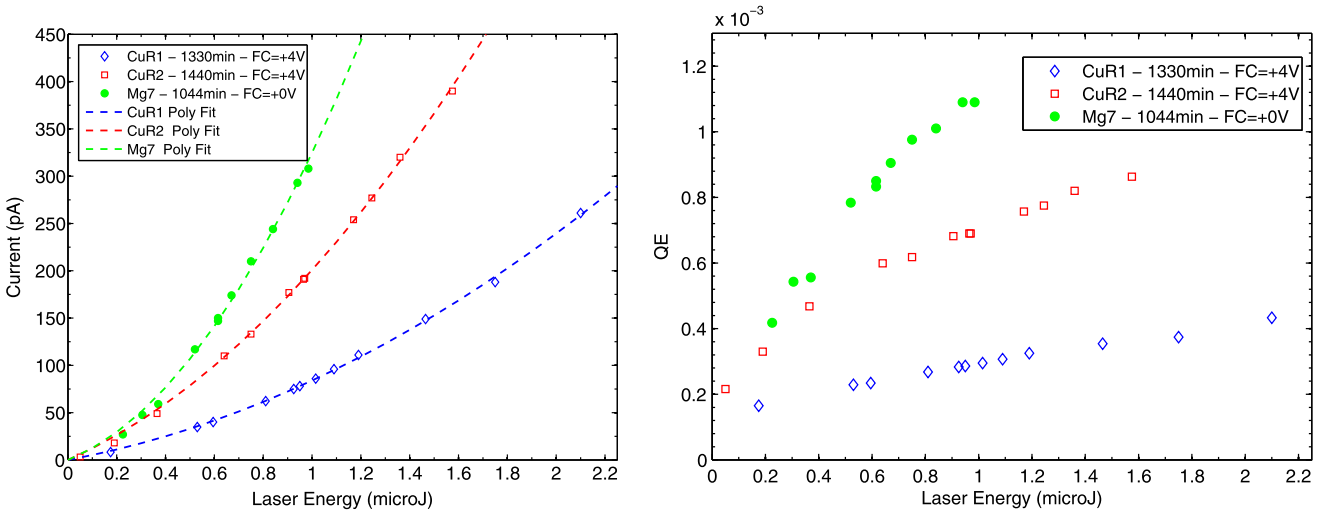

Fig. 14 Current (*left*) and QE (*right*) measured as a function of the Duetto® laser energy for two Cu samples and one Mg *insert*. Two-photon absorption is responsible for electron emission. For Cu the FC is biased at +4 V and is unbiased for the Mg *insert*

5 Aging of various photocathodes: Duetto laser cleaning

The QE evolution of Cu photocathodes when exposed to UV light of high repetition rate lasers and under unbaked vacuum conditions has shown an increase of the QE with time. This is contrary to what is observed in RF photoguns, where long term exposure leads to a drop of QE. Since aging seems not to appear in our experimental conditions, we have investigated laser cleaning, or laser rejuvenation, of cathodes on Cu, Mg, Al, and AlLi photocathodes.

5.1 Cu and Mg

In Fig. 5, at 355 nm, we show the evolution of the QE when the rough polished Mg#2 cathode is exposed to the Duetto® laser light, Fig. 5 (circles). The cathode vacuum chamber was moved from the Topas® laser table to the Duetto® optical table. During this move, the chamber was partially vented to 0.1 mbar of air atmosphere. Despite this venting, the initial QE of the cathode when exposed to the Duetto® laser is similar to the QE measured with the Topas® laser. The laser spot size on the cathode was chosen to be 8 mm in diameter with a fluence of usually 1.2 μJ/cm^2. The fluence per pulse is ∼80 times lower than when using the Topas®. We observed a QE increase with the irradiation time, Fig. 5 data labeled Duetto. At the end of the run, the chamber was moved back to the Topas® table for wavelength tuning; this time without air exposure.

Figure 14 (left) shows the current extracted from two polished Cu cathodes, which were HCl cleaned to remove the oxide layer and then rinsed with alcohol before mounting.

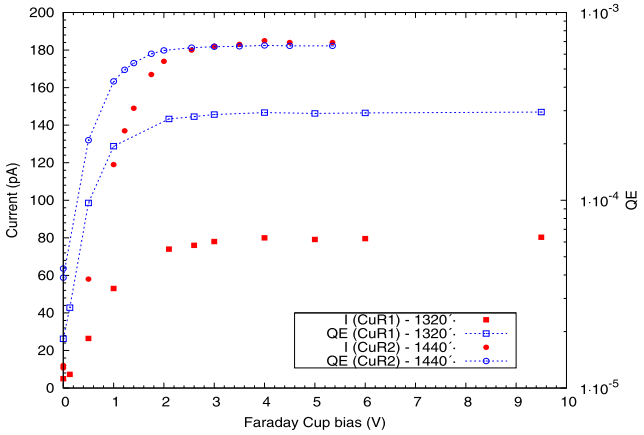

Fig. 15 QE and Current versus the FC bias of two polished mirror-like Cu samples

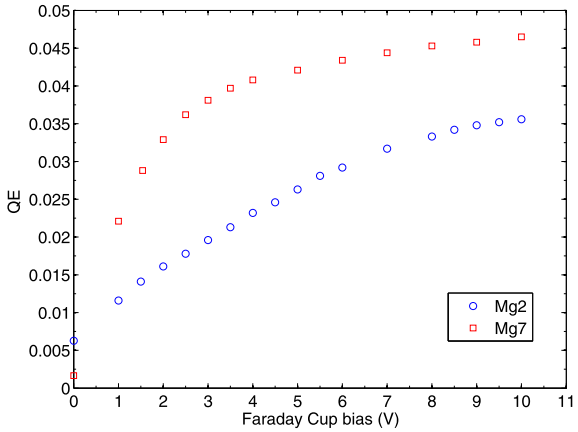

Fig. 16 QE versus the FC bias of two polished Mg sample Mg#2 (rough) and Mg#7 (mirror-like)

Figure 14 also shows the current extracted from a polished and mirror like Mg photocathode (Mg#7) for comparison. The laser peak intensity, associated with the laser energy, varies from 0 to 0.45 MW cm^{-2}. The QE, in function of the laser energy, is shown on the right plot of Fig. 14. For the Cu cathodes, the data plotted were measured while the FC was set to +4 V and 0 V for Mg#7 cathode.

The electron current measured for Cu and Mg while irradiating at 355 nm wavelength, 10 ps pulse length, is due to two-photon absorption, as indicated by a square-law fit of the current vs the laser energy in Fig. 14. We have seen no black marks as in Fig. 8, on either Cu or Mg samples. The samples stayed pristine after a few days of irradiation. The conditioning of Cu was carried out with the Duetto® laser delivering 200 mW of power, while set to 130 mW for Mg#7. With 130 mW (650 nJ/pulse) of laser power, the charge extracted on Cu was small. To improve the charge extraction on Cu, a small +4 V bias was applied in addition to the use of more laser power. The freshly polished Mg gives enough charge at 130 mW of power that it was not necessary to bias the sample. The goal here was to study the evolution in time of the QE for the mirror-like Mg cathode and to compare it (qualitatively) with mirror-like Cu.

Figures 15 and 16 show the effect on the current and QE measured when applying a small positive voltage to the FC. The increase of current extracted is usually above a factor 10 when applying a few Volts on the FC. This shows the effect of the space charge repulsion from the head of a bunch to the extraction of the tail of it.

The total vacuum pressure of the unbaked vacuum system during the laser exposure (2300 min) dropped from 5.1^{-5} Torr to 5.1^{-6} Torr. The evolution of the QE for Cu, goes from the mid 10^{-5} range to the mid 10^{-6} range when the FC power supply is turned off (data not shown). The QE, FC ON, for Cu is ∼0.1 % (Fig. 15) and ∼4.5 % for Mg (Fig. 16). Those QE are much higher than the QE measured for photocathodes installed in an RF photogun. This is explained by the fact that in an accelerator the charge per bunch per laser pulse is accurately measured, hence a correct QE according to the definition. Here, we measure the average current, which we divide by the energy per pulse, hence a different QE definition as already stated at the end of Sect. 2 of this paper.

The volume of interaction between the residual gas and the laser beam is of a few cm^3. At a pressure of 10^{-6} Torr, the density of molecules is in the order of 3×10^{10} cm^{-3} and the number of photons in the beam per pulse is $\sim 2 \times 10^{12}$. The usual cross section of interaction is 10^{-16} cm^2. This would amount to a pA of current, if all ions were falling on the photocathode. Given the amount of charge extracted, the error on the charge measured is negligible, and the QE values quoted are accurate.

The main effect of the FC bias is the suppression of the space charge present at the cathode surface, which hampers the emission of electrons. This space charge is weak enough that only a few Volts are sufficient to counterbalance it, as shown by the current plateau for bias above +4 V, Fig. 15.

We have also monitored the evolution in time of the QE for Mg cathodes when irradiated by the Duetto® at 355 nm, Fig. 17. The laser size on cathode was 8 mm and the repetition rate 200 kHz for all the data plotted. The full diamond plot labeled “Mg2 Jun2010” is the same data plotted in Fig. 5 (open circles). The laser cathode cleaning with low energy per pulse increases the QE by a few orders of magnitude after less than 10 h of exposure. The laser was blocked for 1 h and the system kept under vacuum. Upon restart, the QE barely dropped. The same cathode was reused 6 months later. The cathode was left in the vacuum chamber, which was filled with air and with the vacuum valve closed. After the pump down, the cathode was irradiated with the laser with the same parameters as used previously, including an average power of ∼130 mW; open square data labeled “Mg2 Jan2011.” The QE almost reached the same value as before in the same amount of time. The laser was blocked

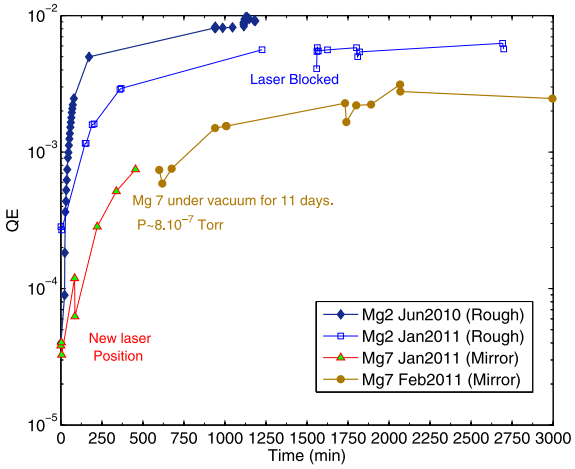

Fig. 17 QE evolution under Duetto irradiation for two polished Mg sample Mg#2 (rough) and Mg#7 (mirror-like). FC is off in all cases

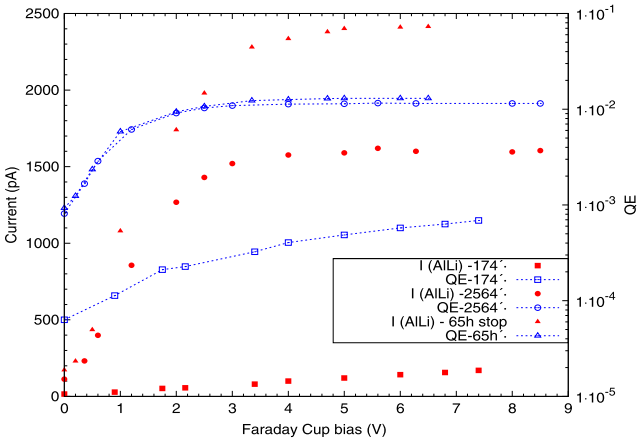

Fig. 18 QE and Current evolution of AlLi alloy during Duetto® exposure as a function of the FC bias voltage

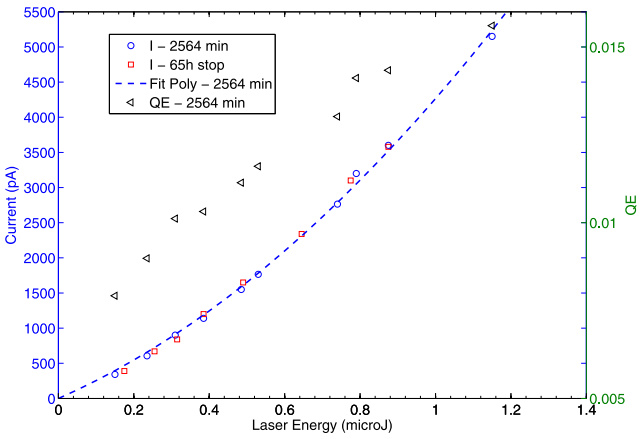

Fig. 19 AlLi Current extracted in function of the Duetto® laser energy. FC is set at +4 V

overnight, with the vacuum pressure improving during the night. Again, the drop in QE was minimal upon resuming irradiation. Damages on the polished but nonmirror-like sample from the irradiation by both lasers have been shown on the left photo of Fig. 8.

A freshly polished Mg (Mg#7) insert was installed in the vacuum chamber, and exposure started when the surrounding pressure was $\sim 5.1^{-5}$ Torr. The parameters used for the irradiation were similar to the ones used for sample Mg#2. The first QE value recorded was lower than for a rougher surface. This is not surprising as rougher surfaces will absorb more photons, hence increasing the production of electrons compared to a flatter surface. The QE of the mirror like surface stays systematically lower than for a rougher surface.

After a couple of hours of irradiation on Mg#7, Fig. 17 (full triangle), the laser spot was moved to another location on the cathode. The sample size was 14 mm and the spot size was 8 mm. It is possible that some overlap with the already conditioned area occurred. This would explain why the QE reduction seen does not fall to the starting value. After a few more hours of laser exposure, the laser was taken away and the system kept in a dynamic vacuum for 11 days. After restart of the illumination (full circle), the QE value of Mg#7 was similar to the end-of-illumination QE value (full triangle), Fig. 17.

It seems to be commonly acknowledged that long exposure to the vacuum residual gas is detrimental to the QE [15]. This result on Mg and some more on Cu (Fig. 13) and AlLi (Fig. 18) is therefore in contradiction with this belief.

Using a high repetition rate, short pulse laser, with a wavelength longer than the associated wavelength of the WF, at a low fluence (less than a microJ of energy per pulse over a "broad" area), in an unbaked vacuum atmosphere has proven efficient in increasing the QE of both Cu and Mg cathodes. In both cases, multiphoton absorption is responsible for electron emission. A quadratic dependence of the current extracted versus the laser energy is the mark of two-photon absorption. In the case of Mg, Mg oxide has a lower work function than pure Mg and the emission at 355 nm is than the usual photoelectric effect, one photon absorption, instead of two-photon absorption. After a few hours of laser exposure, we have not seen any linear dependence of the current extracted versus the laser energy.

5.2 Aluminum and aluminum lithium alloy

Similarly to what was performed on copper and magnesium, we have exposed an aluminum (Al) sample and an aluminum lithium (AlLi) alloy insert to the high repetition rate Duetto® laser.

Al and AlLi photocathode are potential alternatives to Mg as a photocathode. In the Diode-RF electron gun (OBLA), we have measured the emittance and the QE of various metals [14, 16, 46]. With respect to the QE, aluminum has been

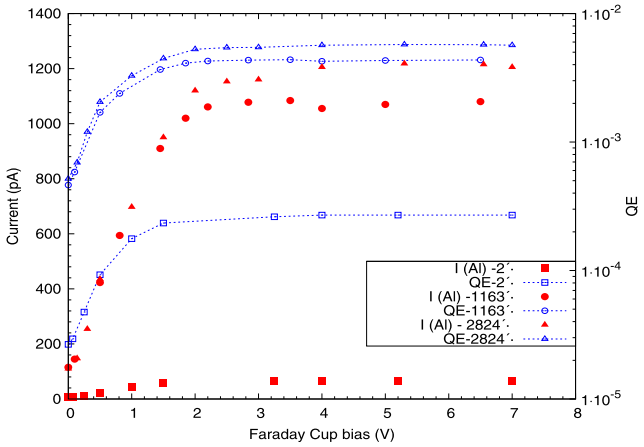

Fig. 20 QE and Current evolution of Al during Duetto® exposition, in function of the FC bias voltage

found better than copper and not as good as magnesium. The emittance was higher than for Cu. According to literature, Mg also produces lower emittance than Cu [17]. What could make Al still attractive is its higher vapor pressure upon baking compared to Mg. Most photo-RF guns are baked before RF processing is started, although the temperature might be less than 150 °C for a long period of time.

An alternative to pure Al as a photocathode material would be to use an AlLi alloy [47]. Lithium and magnesium are in the first and second groups of the periodic table. They are both strongly reactive with oxygen. Both elements may migrate to the surface of Al over time [48]. This may be the reason for the enhanced production of electrons compared to a pure Al surface.

$Al_{95}Li_{2.5}Cu_{1.5}Mg_1$ alloy was bought from Goodfellow® in tube form. The tube was pressed into a circular insert then polished (mirror surface like) and kept in air for 3 months before installation.

The irradiation with the Duetto® laser produced only a few pA of current, independent of the FC voltage, even when using 380 mW of laser power, fluence 3.8 μJ/cm^2. The current extracted did decrease from 3 pA to 1 pA in 20 min. The sample was repolished and reinstalled. The results of the current and QE obtained at different times of exposure versus the FC voltage are shown in Fig. 18.

The production of electrons is done through the two-photon absorption process as seen by the quadratic dependence in Fig. 19. The data labeled "65 h stop" on both figures, Figs. 18 and 19, have been obtained at re-start of irradiation after 65 h of laser downtime. During that time, the chamber stayed actively evacuated by the vacuum pump system. As for Cu or Mg, the QE of the AlLi did not decrease while the sample stayed in an unbaked vacuum ($P \sim 2.6 \times 10^{-6}$ Torr) for a few days.

For extracted current above 1500 pA, during the QE vs. FC voltage scan, and after every step up of the FC voltage the current reads high and can drop by 100 pA in 30 s. For an extracted current below 1500 pA, the current drops by a few pA. After this initial drop in the extracted current, the charge extracted increases slowly again under the Duetto® irradiation. This behavior, where the initial extracted current drops after the laser power has been increased, was not observed on either Cu or Mg.

Finally, we tested a freshly polished Al sample. The QE and current extracted versus the FC bias is shown in Fig. 20 at different times of laser exposure. A previous attempt of measuring the QE vs. wavelength on an Al sample kept in air for a long time did not give consistent results as were obtained for Cu or Mg, Figs. 4 and 5.

Al and AlLi alloy reacted similarly in terms of QE. The initial QE, with the FC unbiased, is in the 10^{-5} range, and increases by a decade at the end of the laser exposure. When turning on the FC, the end value for the QE (for AL and AlLi) is close to a percent. In both cases, the photoemission is two-photon absorption. It seems that for aluminum-based photocathodes, a freshly prepared cathode behaves better than a cathode prepared, and then kept in air for a few months. This was not observed for Mg or Cu. Finally, no damage was seen on either Al or AlLi samples after removal from the chamber.

6 Conclusion

A compact XFEL can only be built if the electron beam emittance is as small as possible. In an XFEL driven by the use of an RF photogun, there is a trade off between the smallest emittance achievable and the quantum efficiency. Measuring the work function of a technical metal photocathode allows not only to characterize the preparation procedure of the cathode but also defines the required gun laser characteristics (wavelength and pulse energy).

In Sect. 3, we have measured the work function of technical metals using an optical parametric amplifier pumped by an infrared laser. We have observed that in the absence of RF and in an unbaked vacuum the QE (or extracted electron current) decreases, but does not drop sharply for wavelengths longer than the work function. This would be what one would expect after measurements made with a powerful UV lamp coupled to a monochromator. Two-photon absorption leading to photoemission was also evident for a UV laser with a longer pulse duration (10 ps) on Al, AlLi, Cu, and Mg; ($\lambda_{Laser} > \lambda_{WF}$). We were not able to determine the cause of the photoemission when using picosecond or shorter laser pulse length, as the emission was space charge affected.

Though laser parameters similar to parameters used for electron production at the PSI photogun were chosen, we did not observe any aging on the cathode tested in our table-top setup. Instead, we observed an increase of the QE in

time which seemed to slowly level off. We attribute this fact primarily to the absence of the RF field. A second reason could be the different vacuum composition between a baked RF photogun, which mainly contains hydrogen, and our unbaked system which predominantly contains water. We hypothesize that the water molecules are cracked by the laser beam on the photocathode and that the radicals produced enhance the QE instead of being detrimental to it. This cracking process is also invoked during the ozone cleaning procedure.

Finally, we have studied the evolution of QE of several cathodes including potential alternatives to Cu, like Mg, Al, and AlLi. In all cases, we have observed that a UV (266 nm and 355 nm) high repetition rate laser (1 kHz or 200 kHz) exposed for hours on various metallic surfaces mounted in an unbaked UHV vacuum environment, results in an increase to the QE. These results are in agreement with the results obtained using aggressive laser cleaning procedures applied to photocathodes for RF photoguns. We observe, contrary to laser cleaning techniques, that the mirror-like polished surfaces stay pristine after our extensive but not intense laser exposure. For Al and AlLi, we have shown that polished cathodes, which were stored in air for months, will not produce any charge even under high laser intensities. For these metals, a final preparation, polishing, or eventually diamond milling, should be carried out immediately prior to the cathode insertion.

Acknowledgements S. Ivkovic for polishing the numerous test samples, often on short notice; the SLS vacuum group and pulse magnet group for equipment and knowledge; the FEMTO group for allowing us to use their lasers during the SLS shutdown; M. Divall for valuable discussion and F. Celli for proofreading this text. F. Ardana-lamas and C.P. Hauri are grateful for support by the Swiss National Science Foundation (grant PP00P2_128493) and SwissFEL. C.P. Hauri acknowledges association to NCCR-MUST.

References

1. R. Ganter, R.J. Bakker, C. Gough, F. Le Pimpec, M. Paraliev, M. Pedrozzi, L. Rivkin, A. Wrulich, Nanosecond field emitted and photo-field emitted current pulses from ZrC tips. Nucl. Instrum. Methods Phys. Res. **565**, 423–429 (2006)
2. K. Togawa, T. Shintake, T. Inagaki, K. Onoe, T. Tanaka, CeB_6 electron gun for low-emittance injector. Phys. Rev. Spec. Top., Accel. Beams **10**, 020703 (2007)
3. Y. Ding et al., Measurements and simulations of ultralow emittance and ultrashort electron beams in the linac coherent light source. Phys. Rev. Lett. **102**, 254801 (2009)
4. F. Loehl et al., High current and high brightness electron sources, in *IPAC2010*, Kyoto, Japan (2010)
5. P. Emma et al., First lasing and operation of an Ångstrom-wavelength free-electron laser. Nat. Photonics **4**, 641 (2010)
6. G. Doumy et al., Nonlinear atomic response to intense ultrashort X rays. Phys. Rev. Lett. **106**, 083002 (2011)
7. B.D. Patterson et al., Coherent science at the SwissFEL X-ray laser. New J. Phys. **12**, 035012 (2010)
8. R. Ganter (ed.), SwissFEL conceptual design report. PSI-10-04 (2012)
9. T. Schietinger et al., First commissioning experience at the SwissFEL injector test facility, in *LINAC10*, Tsukuba, Japan (2010)
10. Time-bandwidth products. http://www.tbwp.com/
11. Amplitude technologies. http://www.amplitude-technologies.com/
12. C. Vicario, R. Ganter, F. Le Pimpec, C.P. Hauri, S. Hunziker, C. Ruchert, T. Schietinger, A. Trisorio, Photocathode drive laser for SwissFEL, in *FEL10*, Malmö, Sweden (2010)
13. A. Trisorio, P.M. Paul, F. Ple, C. Ruchert, C. Vicario, C.P. Hauri, Ultrabroadband TW-class Ti: sapphire laser system with adjustable central wavelength, bandwidth and multi-color operation. Opt. Express **19**(21), 20128 (2011)
14. F. Le Pimpec et al., Results of the PSI diode-RF gun test stand operation, in *IPAC2010*, Kyoto, Japan (2010)
15. A. Lorusso, F. Gontad, A. Perrone, N. Stankova, Highlights on photocathodes based on thin films prepared by pulsed laser deposition. Phys. Rev. Special topics—Accelerators and beams (AB) **14**, 090401 (2006)
16. Workshop on photocathodes for RF guns (2011). http://photocathodes2011.eurofel.eu/
17. H.J. Qian, J.B. Murphy, Y. Shen, C.X. Tang, X.J. Wang, Surface photoemission in a high-brightness electron beam radio frequency gun. Appl. Phys. Lett. **97**, 253504 (2010)
18. Light conversion. http://www.lightcon.com/
19. D.H. Dowell, J.F. Schmerge, Quantum efficiency and thermal emittance of metal photocathodes. Phys. Rev. Spec. Top., Accel. Beams **12**, 074201 (2009)
20. W.M. "Mickey" Haynes (ed.), *Handbook of Chemistry and Physics*, 92nd edn. (CRC Press, Boca Raton, 2012)
21. R.A. Chapman Thermionic work function of thin-oxide-coated aluminum electrodes in vacuum and in cesium vapor. J. Appl. Phys. **35**(10), 2832–2843 (1964)
22. J.A. Assimos, D. Trivich, The photoelectric threshold, work function, and surface barrier potential of single-crystal cuprous oxide. Phys. Stat. Sol. (a) **26**, 477 (1974)
23. F.P. Koffyberg, F.A. Benko, A photoelectrochemical determination of the position of the conduction and valence band edges of p-type CuO. J. Appl. Phys. **53**(2), 1173 (1982)
24. B. Brennan, S. McDonnell, G. Hughes, Photoemission studies of the interface formation of ultrathin MgO dielectric layers on the oxidised Si(111) surface. J. Phys. Conf. Ser. **100**, 042047 (2008)
25. W.F. Krolikowski, W.E. Spicer, Photoemission Studies of the Noble Metals. I. Copper. Phys. Rev. **185**, 882 (1969)
26. D.H. Dowell, F.K. King, R.E. Kirby, J.F. Schmerge, In situ cleaning of metal cathodes using a hydrogen ion beam. Phys. Rev. Spec. Top., Accel. Beams **9**, 063502 (2006)
27. W.E. Spicer, A. Herrera-Gomez, Modern theory and applications of photocathodes. Proc. SPIE Int. Soc. Opt. Eng. **2022**, 18–33 (1993)
28. P. Hofmann Lecture notes on surface science. http://philiphofmann.net/surflec3/surflec011.html
29. Computational electronic structure database (CompES). http://caldb.nims.go.jp/index_en.html
30. J.E. Sipe, J. Becher, Surface-plasmon-assisted photoemission. J. Opt. Soc. Am. **71**(10), 1286 (1981)
31. T. Tsang, T. Srinivasan-Rao, J. Fischer, Surface-plasmon-enhanced multiphoton photoelectric emission from thin silver films. Opt. Lett. **15**, 866 (1990)
32. O. Tüske, Photoémission laser assistée par plasmon de surface. Technical report, CEA Saclay (1997)
33. C. Guo, Surface-plasmon-enhanced photoelectron emission (2010). spie.org/documents/Newsroom/Imported/002935/002935_10.pdf

34. D.Y. Li, L. Wang, W. Li, Effects of grain size from micro scale to nanoscales on the yield strain of brass under compressive and tensile stresses using a Kelvin probing technique. Mater. Sci. Eng. A, Struct. Mater.: Prop. Microstruct. Process. **384**, 355 (2004)
35. P.A. Anderson, A.L. Hunt, Effect of oxygen on the work function of barium. Phys. Rev. **115**(9), 550–552 (1959)
36. M.E. Grubbs, M. Deal, Y. Nishi, B.M. Clemens, The effect of oxygen on the work function of tungsten gate electrodes in MOS devices. IEEE Electron Device Lett. **30**(9), 925–927 (2009)
37. K. Németh, K.C. Harkay, M. van Veenendaal, L. Spentzouris, M. White, K. Attenkofer, G. Srajer, High-brightness photocathodes through ultrathin surface layers on metals. Phys. Rev. Lett. **104**, 046801 (2008)
38. R.J. Cashmann, W.S. Huxford, Photoelectric sensitivity of magnesium. Phys. Rev. **43**, 811 (1933)
39. Q. Yuan, A.W. Baum, R. Fabian, W. Pease, P. Pianetta, Effect of oxygen adsorption on the efficiency of magnesium photocathodes. J. Vac. Sci. Technol., B Microelectron. Nanometer Struct. Process. Meas. Phenom. **21**(6), 2830 (2003)
40. L. Cultreraa, G. Gatti, P. Miglietta, F. Tazzioli, A. Perrone, The role of the adsorbed gases on the photoelectron performance of Mg-based photocathodes. Nucl. Instrum. Methods Phys. Res., Sect. A, Accel. Spectrom. Detect. Assoc. Equip. **587**, 7–12 (2008)
41. R. Paschotta, *Encyclopedia of Laser Physics and Technology* (Wiley-VCH, New York, 2008). http://www.rp-photonics.com/two_photon_absorption.html
42. D.H. Dowell, I. Bazarov, B. Dunham, K. Harkay, C. Hernandez-Garcia, R. Legg, H. Padmore, T. Rao, J. Smedley, W. Wan, Cathode R&D for future light sources. Nucl. Instrum. Methods Phys. Res., Sect. A, Accel. Spectrom. Detect. Assoc. Equip. **622**, 685 (2010)
43. V.G. Tkachenko, A.I. Kondrashev, I.N. Maksimchuk, Advanced metal alloy systems for massive high-current photocathodes. Appl. Phys. B **98**, 839–849 (2010)
44. T. Srinivasan-Rao, J. Fischer, T. Tsang, Photoemission studies on metals using picosecond ultraviolet laser pulses. J. Appl. Phys. **69**, 3291 (1990)
45. R. Ganter. PSI, private communication
46. C.P. Hauri, R. Ganter, F. Le Pimpec, A. Trisorio, C. Ruchert, H.H. Braun, Thermal emittance reduction of electron beam from metal photocathodes. Phys. Rev. Lett. **104**, 234802 (2010)
47. A. Septier, F. Sabary, J.-C. Dubek, A. Boumiz, Une photocathode à réserve alacaline (Al–Li)–Ag–O–Li. C.R. Acad. Sci. Paris **314**(II), 569 (1992)
48. F. Le Pimpec, F. King, R.E. Kirby, Electron conditioning of technical aluminum surfaces: effect on the secondary electron yield. J. Vac. Sci. Technol. A, Vac. Surf. Films **23**, 1610 (2005)